Surface & Coatings Technology 305 (2016) 1–10

Contents lists available at ScienceDirect

Surface & Coatings Technology

journal homepage: www.elsevier.com/locate/surfcoat

Influence of oxygen content on the antibacterial effect of Ag-O coatings deposited by magnetron sputtering

Rita Rebelo [a,b,c,*], S.V. Calderon [b], Raul Fangueiro [a], Mariana Henriques [c], Sandra Carvalho [b,d]

[a] 2C2T, University of Minho, Campus de Azurém, 4800-058 Guimarães, Portugal
[b] GRF-CFUM, University of Minho, Campus de Azurém, 4800-058 Guimarães, Portugal
[c] CEB, Center for Biological Engineering, LIBRO – Laboratório de Biofilmes Rosário Oliveira, University of Minho, Campus de Gualtar, 4710-335 Braga, Portugal
[d] SEG-CEMUC, University of Coimbra, 3030-788 Coimbra, Portugal

ARTICLE INFO

Article history:
Received 31 March 2016
Revised 18 July 2016
Accepted in revised form 21 July 2016
Available online 22 July 2016

Keywords:
Silver microstructure
Silver oxide thin films
Sputtering
Halo tests

ABSTRACT

Ag and AgO_x thin films were deposited by pulsed DC magnetron sputtering, for medical devices, in order to provide antibacterial properties. During the deposition process, oxygen flow, and, consequently, oxygen fraction, was varied (0–15 sccm) to understand the influence of oxygen species in the physical, chemical and structural properties of thin films. Coatings morphology was observed by scanning electron microscopy (SEM) and their nanostructure and composition were assessed by X-ray diffraction (XRD) and X-ray photoelectron spectroscopy (XPS) and energy dispersive spectroscopy (EDS), respectively. XRD and XPS analyses revealed that Ag thin films are composed by metallic Ag, which crystallizes in fcc-Ag phase; whereas AgO_x showed a mixture of Ag_2O and AgO phases for low oxygen fraction that became single AgO with the increase of oxygen fraction in the discharge. Surface wettability and surface tension of the coatings were also determined showing hydrophobic character. Halo inhibition zone tests were performed against *Staphylococcus epidermidis*, in order to evaluate the antibacterial behavior of coatings, and silver ion release was measured. Only AgO_x presented antibacterial behavior, showing that the presence of silver oxide are the main reasons for the antibacterial effect, probably due to the increased production of ROS (Reactive Oxygen Species), making these coatings promising for medical applications.

1. Introduction

Coronary artery disease is the leading cause of death in industrial countries and it is responsible for 70% of angioplasty procedures [1]. Thus, stents assume a major role in the treatment of this disease. These medical devices prevent the blood vessel to be obstructed, by being inserted in human body and keeping the vessel open, reestablishing the normal blood flow [2].

Stents can be fabricated in several materials, such as nitinol, cobalt chromium alloy and stainless steel, being stainless steel most commonly used. Despite all the innovations in stents fabrication, namely the substitution of stainless steel for fibrous materials, including polyester, polytetrafluoroethylene (PTFE) and poly (L-lactic acid) (PLLA) [3], stents still suffer from bacterial colonization, leading to severe infections [4].

Infection in medical devices is very common and it can arise from several sources, such as contaminated surfaces, hands of medical staff, patient own skin or mucus membrane, among others. One of the most common bacteria associated to implant infections is *Staphylococcus epidermidis*, which is a gram-positive bacterium, capable to resist antibiotics and host defenses [5].

In the past years, several developments occurred in order to try to functionalize medical devices with antibacterial properties, through surface modification, with the use of noble metals, like silver, or silver oxides, as coatings on implantable surfaces [6–10]. In fact, the appearance of bacteria with resistant strains to antibiotics leaded to new attempts for resurgence of silver's antibacterial properties [11].

Despite silver being a well-known antimicrobial agent, and having a broad-spectrum of activity, its mechanism of action is not fully understood [5,12]. However, it is suggested that the antimicrobial behavior of silver can be achieved by: 1) the release of Ag^+ ions, 2) the interaction of bacteria with silver nanoparticles and 3) the formation of reactive oxygen species (ROS), as schematized in Fig. 1 [4,9,13,14].

Regarding silver ions, their antibacterial activity is endorsed to morphological and structural damage that ions cause in bacteria. Silver ions can penetrate inside bacteria and cause their lysis, by the inhibition of DNA replication [6,7]. Silver nanoparticles are claimed to be more effective, once present a high surface to volume ration, tending to me more easily ionized. Furthermore, silver nanoparticles can interact directly with bacteria, promoting their death [8,15].

* Corresponding author at: GRF-CFUM, University of Minho, Campus de Azurém, 4800-058 Guimarães, Portugal.
E-mail address: ritarebelo@det.uminho.pt (R. Rebelo).

http://dx.doi.org/10.1016/j.surfcoat.2016.07.064
0257-8972/

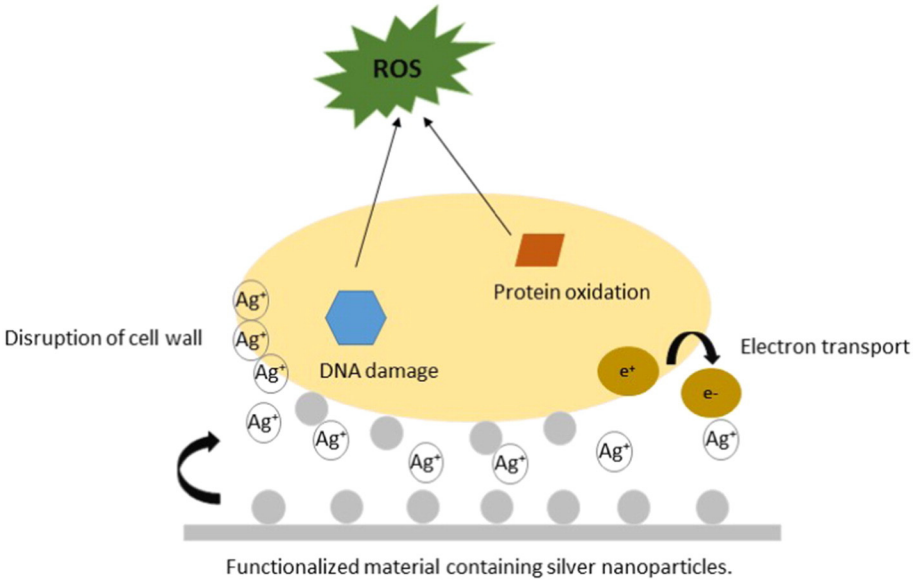

Fig. 1. Schematic representation of mechanism of antibacterial action of silver nanoparticles (adapted from [14]).

ROS can be generated inside or outside the cell and are byproducts of respiring organisms' metabolism. Induction of ROS formation leads to the synthesis of highly reactive radicals that can cause the mitochondrial damage of the microorganism, accelerating the cell death or dysfunction. It is reported that silver can generates ROS, potentially including superoxide (O_2^-), hydroxyl radicals (OH), singlet oxygen ($^1O_2$) and the most stable ROS (H_2O_2) [16].

Therefore, it should be also possible to improve silver antimicrobial characteristics by forming reactive oxygen species, which leads to a most effective antibacterial behavior of silver, due to the toxic character of these species to bacterial cells. For example, Ferreri et al. [5] and Rebelo et al. [8] used oxidized nano-silver and silver oxide thin films, respectively, to achieve antibacterial behavior.

Silver oxides systems have not been well studied, since silver is, generally, consider as a non-reactive material [17]. The Ag-O system presents several defined compounds, such as Ag_2O, Ag_3O_4, AgO and Ag_4O_3, being the Ag_2O and AgO the most stable at high oxygen pressure and low temperature [18,19]. Regarding their synthesis, the most popular method is evaporation of metallic silver following by an oxidation, in a reactive environment (normally, a reactive plasma excited by DC magnetron or microwave), or sputtering [17]. Nevertheless, the report of the application of magnetron sputtering in the formation of silver oxides, and consequently combine the advantages of magnetron sputtering technique and reactive processes [12], has been rarely. The formation of these oxides in form of thin films, depends on the availability of oxygen in the deposition chamber and the energy required for the oxidation, i.e., growth conditions/reaction kinetics [20].

Barik et al. [21], for instance, studied silver oxides prepared by reactive DC magnetron sputtering, operating in constant power mode at 25 W observing that at oxygen flow of 1.71 sccm and 2.01 sccm a stoichiometric Ag_2O (fcc) was formed. Additionally, Raju et al. [20] also evaluated the influence of oxygen partial pressure changes during films growth, by pulsed laser deposition (PLD), revealing that with the increase of the oxygen pressure from 9 to 50 Pa, in the deposition chamber an Ag_2O phase transforms into AgO. In their study, only oxygen pressure was varied, maintained the others growth parameters constant: temperature (300 K), fluence (1.006 J cm^{-2}), substrate-target distance (3 cm) and deposition time (90 min). For an oxygen pressure of 9 Pa, a pure Ag_2O hexagonal crystal system was formed. As chamber pressure increases, an AgO monoclinic crystal system began to appear. For 10 Pa it was observed a mixture of AgO and Ag_2O and for pressures higher than 20 Pa only AgO was formed. Dellasega et al. [22] obtained pure AgO (at higher fluence: 1.6 J cm^{-2}) and conclude the threshold pressure to obtain AgO was 4 Pa. Furthermore, Kumar et al. [19] deposited AgO thin films by RF reactive magnetron sputtering, with a sputtering power of 50 W, at room temperature, with oxygen flow rates from 10 sccm to 30 sccm. The results showed a uniform and stoichiometric AgO (monoclinic crystal system), oriented along the (−111) plane.

However, it is important to evaluate the influence of such changes on the functional properties of the films, namely the antibacterial effect. As a result, the main objective of this work is to produce and characterize silver and silver oxides thin films, by reactive magnetron sputtering, with the main aim of designing a coating that provide antibacterial properties to medical devices such as cardiovascular stents. The oxygen flow variation, during the coatings deposition process, was studied, in order to understand the influence of the oxygen content on the physical, chemical and structural properties of coatings and its effect on the antibacterial activity against *Staphylococcus epidermidis*, probably due to the formation of ROS.

2. Experimental details

Ag and AgO_x coatings were deposited onto stainless steel 316L and silicon substrates by reactive pulsed DC magnetron sputtering. Silicon substrates were used in characterization techniques that evaluate the coatings morphology and structure, while stainless steel 316L substrates were used to evaluate the functional properties. In order to remove impurities and minimize contamination, the substrates were ultrasonically cleaned with distillated water, ethanol and acetone, during 10 min in each solution, before deposition. Additionally, the substrates and the silver target (200 × 100 mm^2) were cleaned by an argon plasma etching process prior to each deposition. The etching process was performed in an argon atmosphere (80 sccm), using a pulsed DC power supply at 0.4 A, 1536 ns of reverse time and 200 kHz applied to the substrate holder and a DC power supply, with a current density of 0.5 mA cm^{-2}, applied to the Ag target.

During the deposition process, the sputtering atmosphere consisted of a constant argon flow (60 sccm) and an O_2 flow that varied from

0 scmm to 15 sccm, (increasing 1.5 sccm per deposition), corresponding to a variation in the fraction of oxygen in the discharge ($fO_2 = \Phi O_2 / (\Phi O_2 + \Phi Ar)$ from 0 to 0.2. Total pressure inside the chamber varied from 5.8×10^{-1} Pa until 7.8×10^{-1} Pa, with the increase of the O_2 flow. A pulsed DC power supply was connected to the silver target, applying a current density of 1 mA cm^{-2}, and the reverse time and the frequency were kept at 1536 ns and 200 kHz, respectively. The samples were placed in a substrate holder, located 70 mm away from the target and rotating at a constant velocity of 7 rpm. The deposition time (8 h) was maintained constant for all the coatings. Deposition process was performed at room temperature.

XPS (X-ray photoelectron spectroscopy) analysis was performed on coated silicon, in order to obtain information about binding state of the samples. The analysis was made using a Kratos AXIS Ultra HSA equipment, with VISION software for data acquisition, carried out with a monochromatic Al Kα X-ray source (1486.7 eV), operating at 15 kV (90 W), in FAT mode (Fixed Analyser Transmission), with a pass energy of 40 eV and a pass of 0.1 eV for regions ROI and 80 eV and a pass of 1.0 eV for survey. A charge neutralization system was used and the data acquisition was performed with a pressure lower than 1×10^{-6} Pa. Data analysis was performed by CasaXPS software and the effect of electric charge was corrected by the reference of the carbon peak (285 eV).

The morphology and thickness of the coatings deposited on silicon, were evaluated by scanning electron microscopy (SEM) in a NanoSEM – FEI nova200 equipment, being analyze three different regions, but only present a representative micrograph. Energy dispersive spectroscopy (EDS) was performed for the detection of coatings bulk composition.

Structure and phase distribution of coatings was assessed by X-ray diffraction (XRD) analysis in a PANalytical X'Pert PRO MPD system, using CuKα (λ = 0.154056 nm) radiation (45 kV and 40 mA) with a parallel beam configuration, in a grazing incidence mode with an angle of incidence of 5°. A voigt function was used for fitting the XRD peaks, calculating the peak position (2θ) and the full-width at half-maximum (fwhm), with the intuit to calculate the grain size.

Contact angle measurements were performed with the view to investigate the samples hydrophobic behavior, using the van Oss approach, in 6 samples of each coating, through the sessile drop contact angle technique, using an automated contact angle measurement apparatus (OCA 15 Plus; Dataphysics, Germany). For this purpose, water, formamide and α-bromonaphthalene were used, in order to evaluate fluids with different values of surface free energy, Υ_l^{Tot}; apolar Lifshitz–van der Waals surface free energy component, Υ_l^{lw}; electron acceptor surface free energy component, Υl^+; and electron donor surface free energy component, Υl^-. For statistical analysis, one- way ANOVA analysis was used, by applying Tukey multiple comparisons test, using the software Statistical Package for the Social Sciences Inc. (SPSS). All tests were performed with a confidence level of 95%.

Halo inhibition zone tests, against *Staphylococcus epidermidis* (IE 186), were performed in order to evaluate, as a qualitative measure, antibacterial activity. A colony of *S. epidermidis* was taken from Tryptic Soy Agar (TSA, Merck), 20 ml of Tryptic Soy Broth (TSB, Merck) was added and incubated for 18 h, at 37 °C and 120 rpm. A volume of 1 ml of 1×10^7 CFU·ml^{-1} cellular suspension was added to 14 ml of TSA and placed in sterile Petri dishes. The different coatings were placed in Petri dishes and incubated, during 24 h, at 37 °C. The halo formed around the coatings, deposited on steel, after 24 h, was measured. All the assays were run in triplicate.

Ag ion release tests were performed by immersing the samples in 50 ml of NaCl 0.9%, over a 24 h period. A volume of 2 ml of the solution was taken from the samples and added to 4 ml of HNO_3 5%. The release of Ag ions was measure using a PERKINELMER, ICP-OES OPTIMA 8000, with a 6106PE POLYSCIENCE refrigerator and a S10 PERKINELMER automatic sampler. All the tests were run in triplicate.

3. Results and discussion

3.1. Coatings deposition

Silver oxide coatings deposited in reactive sputtering mode were labelled as AgO following by the percentage of O_2 flow used in the deposition. Thus, AgO10 corresponds to a deposition with 10% of the total O_2 flow (1.5 scmm); AgO20 corresponds to a deposition with 3 sccm of O_2 flow, etc.

Fig. 2 shows the variation of Ag target voltage and pressure in deposition chamber according with the fraction of oxygen. It reveals that the target voltage increases up, with a tendency to stabilize, from 86.9 V up to 92.4 V.

As the fO_2 increased, an increase in the total pressure and in the silver target voltage is observed, once the reactive gas is not totally consumed during the growth of thin films, which leads to a formation of a compound (Ag-O) in the target surface, associated with a variation in effective secondary electron emission yield (SEEY), reaching a poisoned mode. In this study, the silver oxide coatings were deposited with a fO_2 of 0.2, in a poisoned mode.

The deposition rate of the films (see Fig. 3) was calculated from the thickness (observed by SEM) and deposition time, revealing an increase for the film deposited with the lowest fraction of oxygen and continuously decreasing as oxygen is incorporated. This behavior is attributed to the introduction of oxygen, which in an initial phase, contributes along with silver to films growth, leading to an increase of deposition rate with the introduction of oxygen. However, for higher amounts of oxygen, silver target is poisoned with oxygen, leading to deposition of silver oxides, and, consequently, to lower deposition rates, once silver oxides have lower sputtering yield, when compared with pure silver [23]. The low deposition rate of Ag was not verified in previously studies [8], which can indicate that the target intensity applied can be in the limit of operation.

3.2. Chemical, morphological and structural analysis

A bulk composition of the coatings was performed by EDS analysis, indicating an excess of silver for AgO10 and AgO20 coatings, while for the remaining coatings the amount of silver and oxygen are similar, suggesting an AgO composition (Fig. 4).

Figs. 2 and 4 reveal that with the increase of the fraction of oxygen in the discharge, the pressure in the chamber increases linearly in the entire range of oxygen fraction. The increase of oxygen also leads to an increment in the Ag target voltage, but the voltage stabilizes, approximately after $fO_2 = 0.09$. The same tendency is observed in atomic composition of the coatings, where the percentage of oxygen increases, until $fO_2 = 0.09$, stabilizing after that.

In Table 1, the Ag/O ratio of silver oxide coatings is summarized, as well as oxygen fraction in the discharge and O_2 partial pressure and the O_2 flow uses to obtain those ratios.

SEM results (Fig. 5) suggest the presence of a compact film in Ag coating contrary to AgO_x coatings that present some porosity. AgO_x coatings show a more columnar structure, compared to the pure Ag coating; however the increase of oxygen fraction minimizes the porosity, producing more compact films and with lower column size. However, after $\Phi O_2 = 0.13$ the thin films are compact.

In order to obtain a more detailed information about the coatings structure, XRD analysis was performed. The XRD diffraction patterns of Ag, AgO10, AgO20, AgO40, AgO60, AgO80 and AgO100 coatings are presented in Fig. 6. The XRD spectrum evidenced three different structure in the films. The Ag films with a typical face-centered cubic (FCC) structure (ICDD card no 00-004-0783), polycrystalline with randomly oriented crystallites and grain sizes of 78.5 nm, calculated by Scherrer formula.

For AgO_x films, on the other hand, two distinctive behaviors are noticed. For large oxygen fractions (AgO40 to AgO100), a pure monoclinic

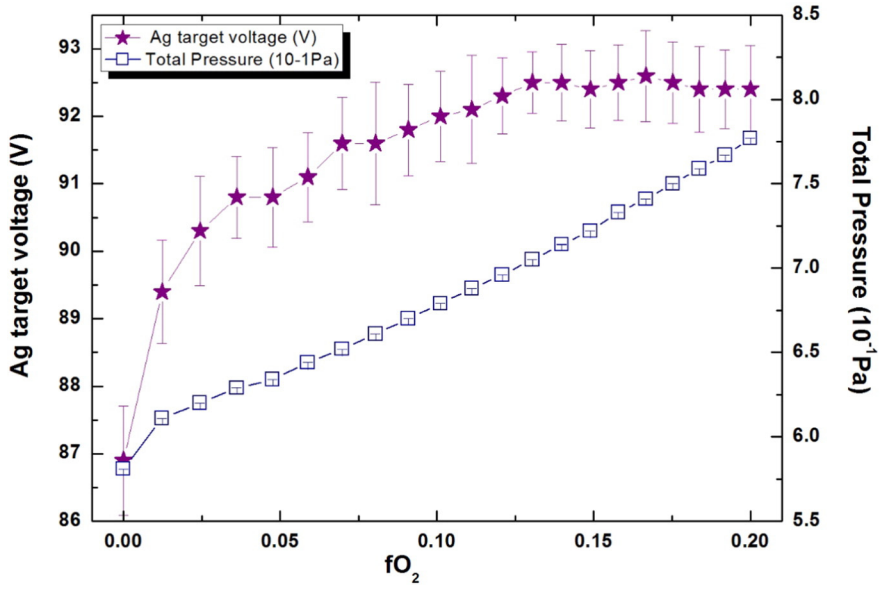

Fig. 2. Variation of Ag target voltage and total pressure in deposition chamber for different oxygen fractions in the discharge.

AgO phase is easily identify (ICDD card no 00-043-1038), which is in agreement with the composition of the films, where the ratio between Ag and O is close to the unit, as previously discussed. Nonetheless, for low oxygen fractions (AgO10 and AgO20) at least two scenarios can be considered. In the first case, a pure monoclinic AgO phase was fitted (ICDD card no 00-043-1038), where residual stresses in the films may slightly increase the lattice parameter. This variation results in a shift of the (002) plane towards lower angles. The simulation predict a variation from 0.549 to 0.559 nm, in the lattice parameter, which is likely to occur for grains preferentially orientated in the (002) direction and films in compressive stress. These results can simulate the spectra obtained for sample AgO10. Yet, there is still a lack of fit for AgO20, where the diffraction peak corresponding to 56.3° is not included in the fitted spectrum, as shown in Fig. 7a). Additionally, pure AgO phases would not explain the excess of silver in those films.

As a result, a second scenario is proposed, considering a mixture of Ag_2O FCC (ICDD card no 00-043-0997) and monoclinic AgO phases and the result are shown in Fig. 7b). In this case, the diffraction occurring at 56.3° is included as the (022) diffraction of the Ag_2O phase, decreasing the fitting deviation. However, the cell parameter for the cubic structure showed a slight deviation from the theoretically value, showing a difference of 0.009 nm (from 0.471 nm to 0.463 nm). This variation may be due to the lack of stoichiometry of the compound, where instead of pure Ag_2O, an Ag_xO phase is formed. This has been previously reported in silver oxide nanostructures [24].

Considering the previous analysis, silver oxide coatings AgO10 and AgO20 are identified as a mixture of sub-stoichiometric Ag_xO fcc phase, with composition close to Ag_2O, and AgO monoclinic phases. For higher oxygen fractions (AgO40 to AgO100), Ag_2O disappears and coatings only present a single AgO monoclinic phase. These results are in agreement with the composition of the films, where for high oxygen fractions there is sufficient oxygen to form a pure AgO compound, as previously mentioned. The difference observed in silver oxides, with the increase of oxygen fraction, can be justified by the availability of oxygen in the reaction zone, resulting in the formation of different valence states of metal oxide [20].

As reported above, Ag is present in a form of a compact thin film with a nanocrystalline structure, with a grain size of 78.5 nm. AgO_x coatings show a thin film with some porosity and a more columnar structure, compared to the pure Ag coating; however the increase of O2 flow minimizes the porosity, producing more compact films and with lower column size. From Fig. 3 it is possible to calculate the thickness of coatings, which are presented in Table 2.

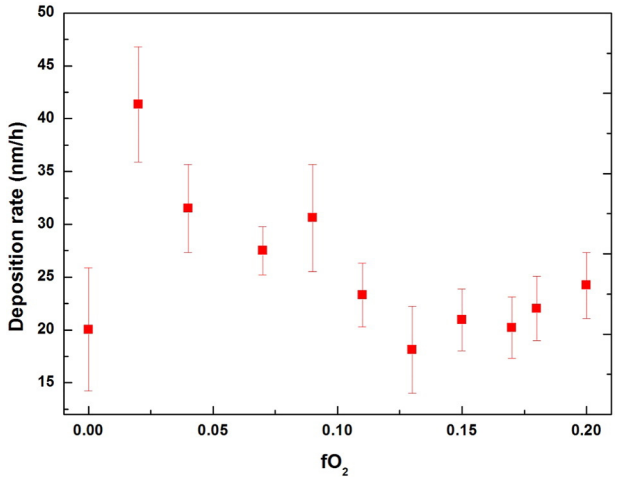

Fig. 3. Variation of deposition rate for different oxygen fractions in the discharge.

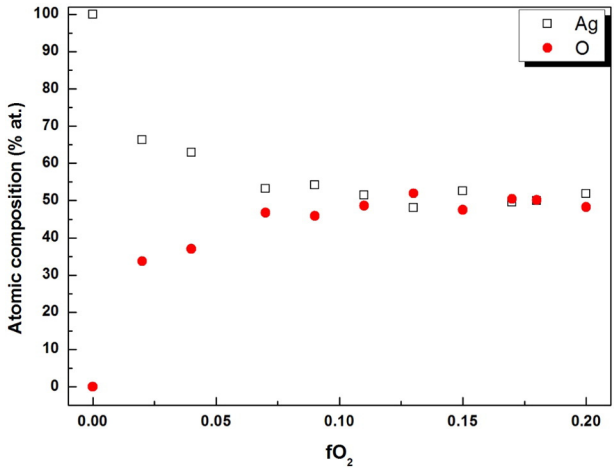

Fig. 4. EDS composition for silver oxide coatings.

Table 1
Ratio of Ag/O composition of silver oxide coatings.

Nomenclature	% O_2 flow	O_2 flow (sccm)	pO_2 (Pa)	$fO_2=\frac{\Phi_{O2}}{\Phi_{Ar}+\Phi_{O2}}$	Ag/O ratio
AgO10	10	1.5	9.35	0.02	2.0
AgO20	20	3	13.6	0.04	1.7
AgO30	30	4.5	17.2	0.07	1.1
AgO40	40	6	19.5	0.09	1.2
AgO50	50	7.5	21.3	0.11	1.1
AgO60	60	9	26.0	0.13	0.9
AgO70	70	10.5	28.4	0.15	1.1
AgO80	80	12	29.7	0.17	1.0
AgO90	90	13.5	31.2	0.18	1.0
AgO100	100	15	28.6	0.20	1.0

According to Fig. 2 and the compositional, structural and morphological results presented, four samples were chosen to continue the study of chemical bonding and antibacterial characterization (Ag, AgO10, AgO20 and AgO100). The remaining samples were discarded for further analysis due to their similar composition, morphology and structure with samples AgO100.

In order to confirm the chemical state and binding energy of the coatings surface and the phase composition, XPS analyses were carried out. Nevertheless, XPS analysis of silver and silver oxides is very complex, once the binding energies of metallic silver and its oxides are reported with low dispersion of values, or even superposition.

In order to facilitate the identification of oxidation states, the Auger Parameter (AP) was used, since it is considered to be more reliable that finding the correct binding energy of each state of oxidation [25]. AP does not depend on the sample charge shift, avoiding charge correction, and AP peaks present larger chemical shifts than photoelectron peaks [25]. Despite the fact that this parameter allows distinguishing the reduced form Ag^0 from its oxidized forms, it cannot distinguish Ag (I) form from other oxidation states, and thus other parameter such as the FWHM of the peak should be considered. Hence, XPS analysis of coatings were carried out with binding energy for Ag 3d and kinetic energy for Ag MNN, as observed in Fig. 8. The bonding types, binding energies, APs and possible structures are summarized in Table 3.

For Ag coating, the spectra suggest the presence of a doublet with the Ag 3d5/2 peak located at 368.86 eV. This fact, combined with auger parameter, is reported to correspond to Ag—Ag bond in metallic state [26,27]. On the other hand, Ag—O bonds at 368.28 eV [1], for transition mode coatings (AgO10 and AgO20), and at 368.31 eV for the coating in the reactive mode (AgO100). These binding energies are compatible with silver oxides. According to Ferraria et al. [25], the doublet assignable to Ag 3d have different characteristics in AgO, Ag_2O and

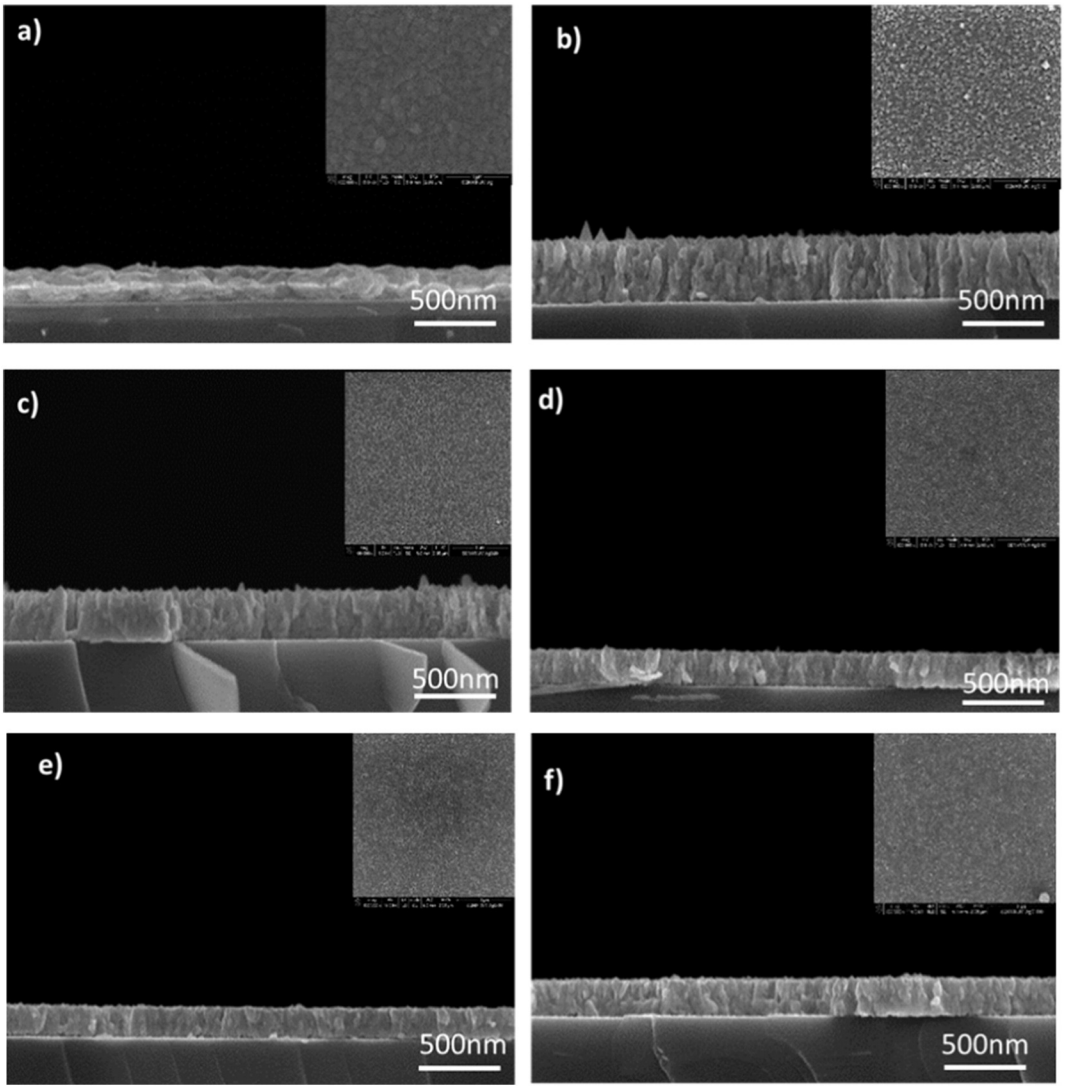

Fig. 5. SEM films cross section detailed view (recorded in SE mode at 100 kX) and top-view micrographs (recorded in SE mode at 100 kX) (a) to (f) referent to Ag, AgO10, AgO20, AgO50, AgO80 and AgO100, respectively.

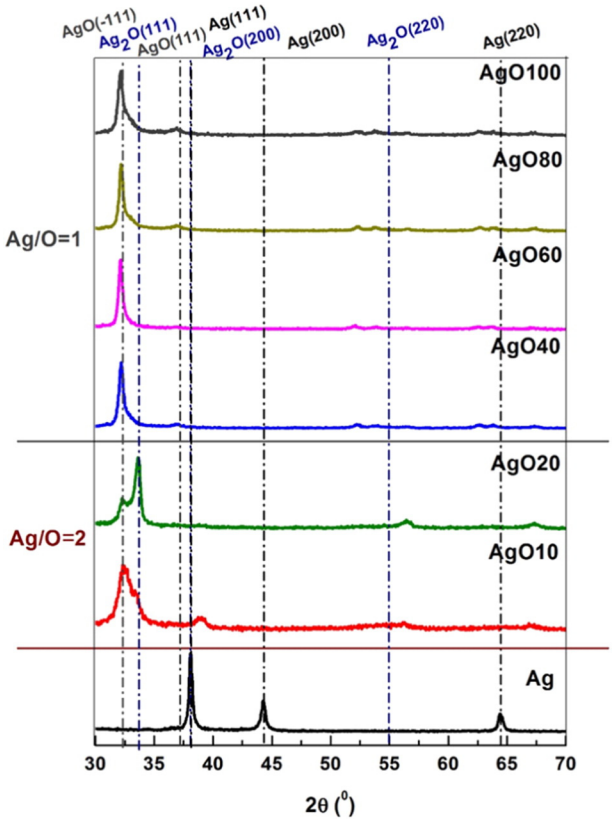

Fig. 6. XRD patterns of Ag and Ag_xO coatings, according to ratio of Ag/O composition obtained by EDS.

in a mixture of those two phases, regarding binding energy and FWHM. In fact, the Ag 3d doublet, reported in such study, is slightly shifted in

Table 2
Thickness of silver and silver oxide coatings.

Sample	Thickness (mn)
Ag	159.6
AgO10	328.9
AgO30	218.6
AgO40	242.2
AgO50	185.2
AgO60	146.2
AgO70	166.3
AgO80	162.7
AgO90	175.4
AgO100	195.3

AgO coating (0.4 ± 0.1 eV) and presents the largest FWHM, when compared with a mixture of Ag_2O and AgO powders [25]. This behavior is observed in sample AgO100, when compared to AgO10 and AgO20 coatings, as shown in Fig. 8,supporting the idea of a mixture of AgO + Ag_2O phases for AgO10 and AgO20 coatings and a single AgO phase for AgO100 coating, observed by XRD, and corroborated by compositional analysis.

Furthermore, XPS spectra to O 1s and C 1s are presented in Fig. 9. Some residual oxygen and carbon are associated with surface contamination, since no previous sputter cleaning was performed in order to avoid preferential sputtering of O and any structural damage in the coatings. Additionally to the contamination, O-Ag peak (529.3 eV), associated to the bonding of silver oxide, was identified in the AgO_x coatings, which has been reported to shift to lower binding energies for pure AgO phases, observed in AgO100 coating, when compared with Ag_2O and their mixture [25].

3.3. Surface properties

The measurement of contact angle allows the evaluation of the hydrophobicity character of a surface. When the variation of the free

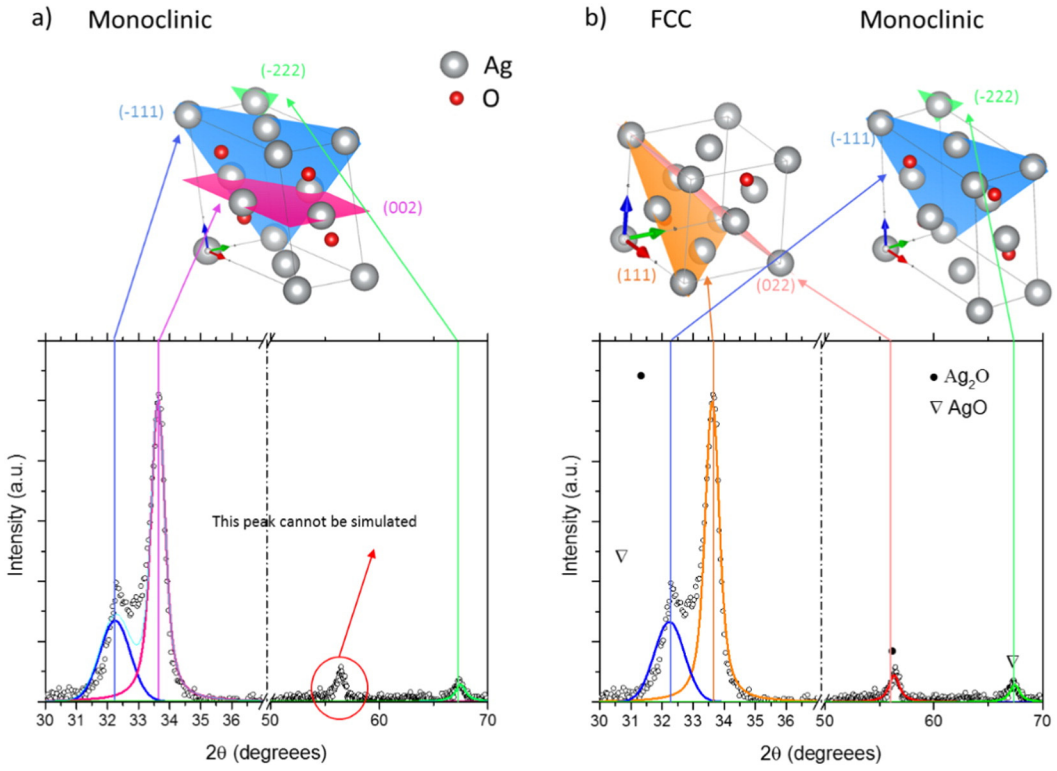

Fig. 7. a) AgO20 XRD pattern fitted using a monoclinic AgO structure, b) AgO20 XRD pattern fitted using a mixture of Ag2O and AgO phases. The symbols correspond to the experimental results and the color lines to the fitted lattice plane identified structures.

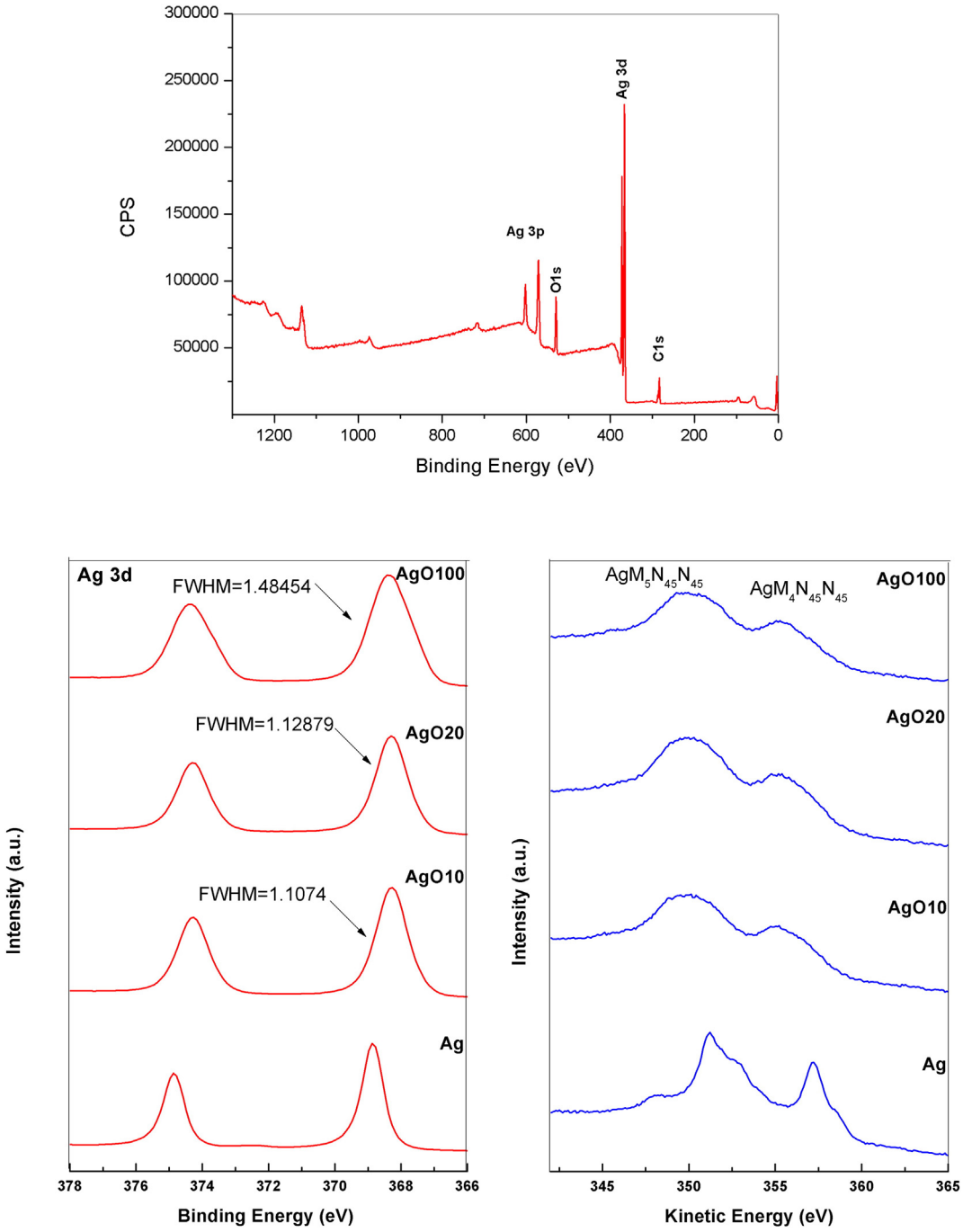

Fig. 8. XPS survey spectra and detailed regions of Ag 3d (left) and Ag MNN (right) for Ag and AgO_X thin films.

energy of interaction (ΔG) between the material's surface (Δm) immersed in water (ΔG_{mwm}) has a negative value, the material is hydrophobic, which means a higher interaction between the material molecules than with water. For hydrophilic materials, this variation of energy assumes a positive value. The contact angle with water also allows to evaluate the hydrophobicity of a given surface, where contact angles above 90° corresponds to hydrophobic surfaces, while lower contact angles correspond to hydrophilic surfaces [9].

Table 4 shows the contact angles, surface energy parameters and degree of hydrophobicity of all the coatings. The results evidence that all coatings present a hydrophobic surface, since the water contact angles are above 90° and ΔG_{mwm} present negative values. Ag100O coating is statistically different from the others ($p < 0.05$).

Additionally, all coatings present a monopolar surface. Higher density of apolar areas in material's surface promote can promote an attachment of microorganism via the hydrophobic effect, due to the increment of hydrophobic interactions [28].

Table 3
XPS analysis of different coatings [1–4].

Coating	Bonding	Binding Energy (eV)	Auger parameter (eV)	Compatible with
Ag	Ag—Ag	368.86	726.09	Ag
AgO10	Ag—O	368.28	723.36	AgO/Ag_2O
AgO20	Ag—O	368.28	723.41	AgO/Ag_2O
AgO100	Ag—O	368.31	723.37	AgO/Ag_2O

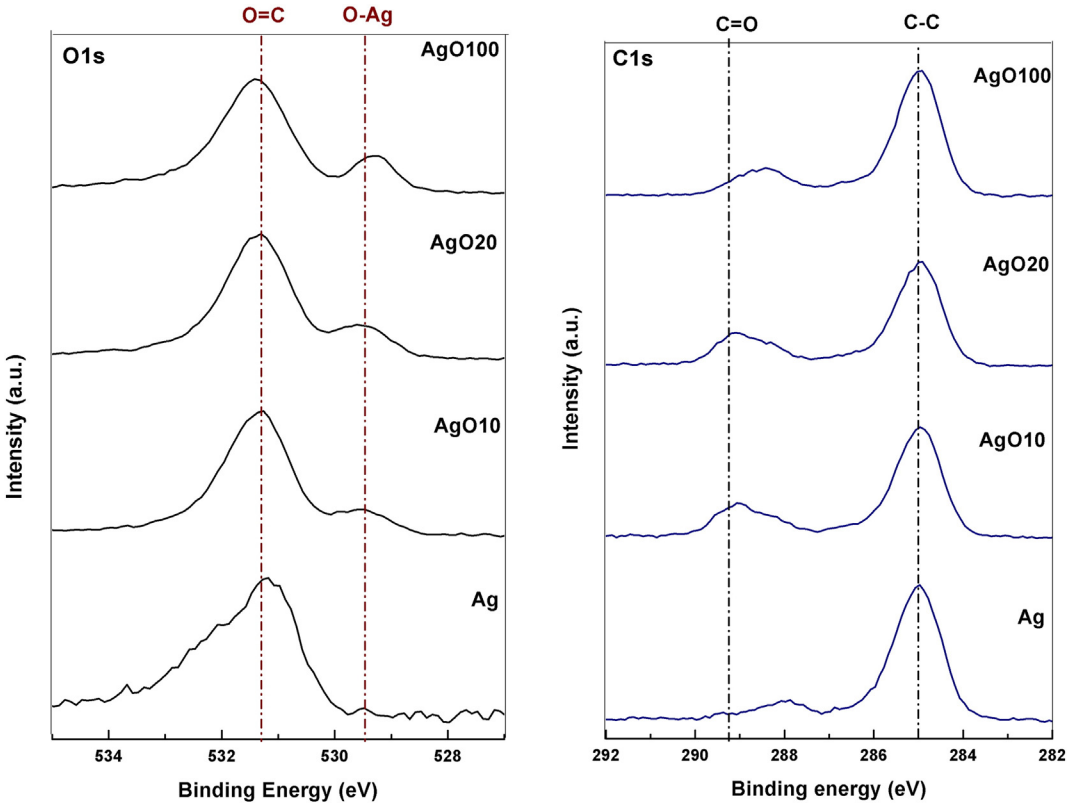

Fig. 9. XPS O1 (left) and C 1s (right) spectra for Ag and AgO_x thin films.

Table 4
Water (Θw), formamide (ΘF) and α-bromonaphtalene (Θα-B) contact angles, surface energy components (apolar Lifshitz-van der Waals surface free energy component, γ^{lw}; electron acceptor surface free energy component, γ^{+}; electron donor surface free energy component, γ^{-}.

Coating	Contact angle ± S.D.(°)			Surface energy components (mJ/m^2)			ΔG_{mwm} (mJ/m^2)
	Θ_w	Θ_F	$\Theta_{\alpha\text{-}B}$	γ^{lw}	γ^{+}	γ^{-}	
Ag	102.4 ± 0.7	95.4 ± 1.8	52.6 ± 0.5	28.7	0.0	5.1	−57.2
AgO10	101.1 ± 2.7	88.4 ± 6.1	44.5 ± 1.5	32.6	0.0	3.3	−67.7
AgO20	99.4 ± 3.6	88.6 ± 0.8	40.5 ± 0.7	34.4	0.0	4.4	−62.6
AgO100	107.1 ± 1.7	90.3 ± 3.0	50.1 ± 2.7	29.9	0.0	1.1	−82.2

3.4. Antibacterial properties

Halo inhibition tests were performed in order to evaluate the existence of antibacterial properties of the coatings, against *Staphylococcus epidermidis*. The results obtained are present in Fig. 10. A halo zone (zone of inhibition of bacteria growth) in oxide coatings is clearly observed. On the other hand in Ag coating the halo is not visible, which means the pure Ag continuous film did not present antibacterial activity against *S. epidermidis*.

As previously suggested, the form of silver can influence the antibacterial efficiency. The presence of Ag nanoparticles tends to ionize more easily, when compared with a compact film, and also interact, directly, with bacteria, promoting their destruction [15]. Once in studied coatings there is no evidence of silver nanoparticles, the antibacterial

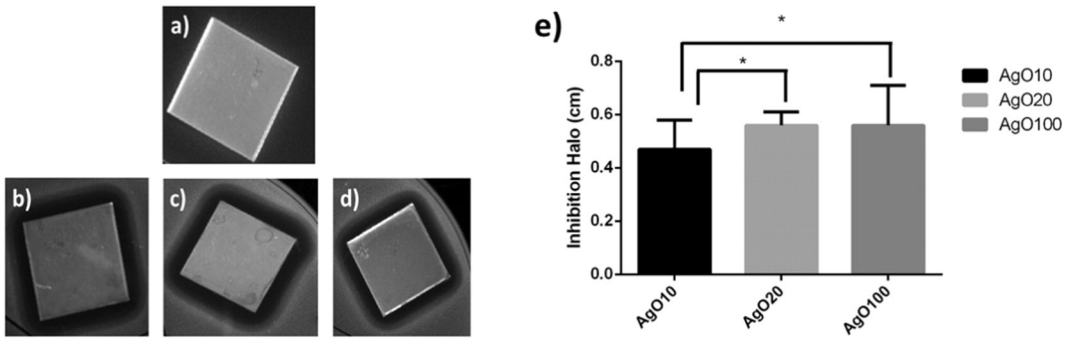

Fig. 10. Results of antibacterial tests for: Ag (a); AgO10 (b); AgO20 (c) and AgO100 (d) and halo size (e) for all coatings. The data are expressed as mean ± standard deviations. One way ANOVA was used with significant level of 95% (*$p < 0.05$).

behavior of the silver oxide coatings should be due to a higher silver ion release of those coatings, when compared with pure Ag coatings or due to an increase of ROS production induced by those coatings.

Previous studies [8] showed that in silver thin films, Ag ionization is insufficient or non-existent and, consequently, no antimicrobial activity was observed. Nevertheless, the silver morphology (nanoparticles (NP's); clusters or films) seems to influence the antimicrobial behavior [11], in many cases correlated to the changes in silver ionization in different morphologies. However, it has been also proposed that silver nanoparticles generate more ROS than silver ions [29], which means that it is the specific characteristics of silver morphology the main responsible for the production of ROS and that it is not the presence of Ag^+, but the process of their release, the main cause of ROS formation [14]. This species has been correlated to antibacterial behavior of silver.

For the analysis of Fig. 4 it is possible to observe that silver at.% decreases until fO2 = 0.11 (corresponding to AgO50), remaining, approximately constant (at.%50) after that. For higher fO2, silver at.% takes the value of: approximately, 70, for fO2 = 0.02 (AgO10), approximately, 60 for fO2 = 0.04 (AgO20), approximately, 53 for fO2 = 0.07 (AgO30) and, approximately, 54 for fO2 = 0.09 (AgO40). Furthermore, in order to understand the main cause of antibacterial behavior present in silver oxide coatings, ICP-OES was performed after 24 h period of contact of coatings with NaCl 0.9%. In Fig. 11 it is possible to analyze the Ag^+ release from coatings and it is possible to observe that silver oxides did not presented a higher silver ion release, which means that is not the amount of silver ions the key factor in the achievement of antibacterial properties presented by silver and silver oxides coatings.

According with ICP-OES and halo tests results, it is suggested that the formation of ROS is, probably, the agent responsible for the antibacterial properties of silver oxides.

Ninganagouda et al. [30] demonstrated that Ag nanoparticles when in contact with bacteria inhibited their growth, due to ROS formation. However, when it was added an antioxidant to Ag nanoparticles, the antibacterial behavior was not observed. This study determined that the antioxidant agent prevented the formation of a silver oxide layer on Ag nanoparticles' surface, and consequently, inhibited the antibacterial activity. Thus, the use of a silver oxide coating can be an advantage in ROS formation and explain antibacterial results.

Furthermore, as demonstrated by Ferreri et al. [5], the incorporation of oxidized silver on coatings can inhibit the bacterial growth, since allows the synthesis of OH^- in aqueous environments (Eq. (1)).

$$Ag_2O + H_2O \leftrightarrow 2Ag^+ + 2OH^- \quad (1)$$

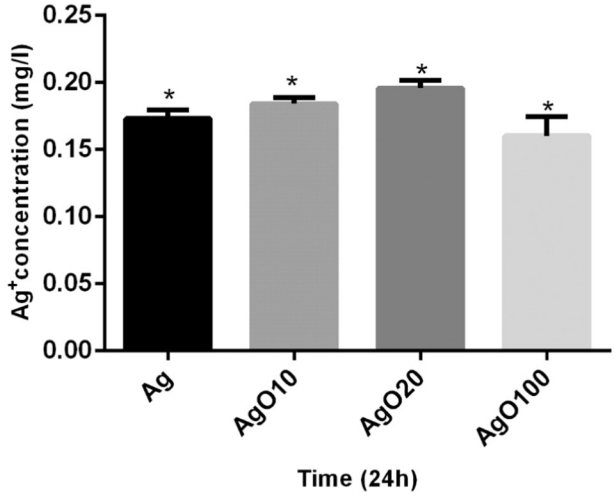

Fig. 11. Results of ICP-OES test. The data are expressed as mean ± standard deviations. One way ANOVA was used with significant level of 95% (*p < 0.05).

Antibacterial tests demonstrated that the formation of reactive oxygen species could be the principal motive to achieve antibacterial properties, since silver oxide coatings presented antibacterial activity unlike continuous silver coating.

Beside antibacterial properties, coatings' cytotoxicity was evaluated, through MTS assays, and AgO100 did not present cytotoxicity, which makes these coating suitable to medical applications. These results open the possibilities to pursue more exhaustive biological studies, which will be detailed in a posterior work.

4. Conclusions

Ag and AgO_x coatings were deposited by non-reactive and reactive pulsed dc magnetron sputtering, respectively. The O_2 flow and, consequently, oxygen fraction during the deposition process, was varied in order to evaluate the influence of oxygen species in coatings properties.

The structural and morphological characterizations revealed that, Ag coating forms a continuous layer, composed by crystalline fcc-Ag phase. The incorporation of oxygen in the deposition atmosphere lead to the formation of a coating composed by a mixture of Ag2O + AgO phases. As the amount of oxygen fraction increase, the observed thin film became, only, AgO, with a monoclinic crystalline phase.

Halo inhibition testes revealed the antibacterial behavior of AgO_x coating unlike Ag coating. The differences on coating behavior may be attributed to film composition (the incorporation of oxygen leads to a higher formation of ROS and, consequently, to an antibacterial behavior).

The obtained results suggest that AgO_x coating, deposited by DC magnetron sputtering has potential to be used in biomedical applications, such as surgical instruments.

Acknowledgments

The authors acknowledgments the financial support of FCT-Fundação para a Ciência e Tecnologia through grant SFRH/BD/90321/2012.

Also thank support by FEDER through the COMPETE Program and by the Portuguese Foundation for Science and Technology (FCT) in the framework of the Strategic Funding UID/FIS/04650/2013, and projects ERA-SIINN/0004/2013 through the "Fundo Europeu de Desenvolvimento Regional" (FEDER).

References

[1] L.H.G. França, A.H. Pereira, Update on vascular endoprostheses (stents): from experimental studies to clinical pratice, J. Vasc. Bras. 7 (2008) 351–363, http://dx.doi.org/10.1590/S1677-54492008000400010.
[2] N. Vila, Braided Hybrid Stents Design, 2009, http://dx.doi.org/10.1017/CBO9781107415324.004.
[3] B. O'Brien, W. Carroll, The evolution of cardiovascular stent materials and surfaces in response to clinical drivers: a review, Acta Biomater. 5 (2009) 945–958, http://dx.doi.org/10.1016/j.actbio.2008.11.012.
[4] L.R. Rodrigues, Inhibition of bacterial adhesion on medical devices, Exp. Med. Biol. 715 (2011) 351–367, http://dx.doi.org/10.1007/978-94-007-0940-9.
[5] I. Ferreri, S. Calderon, V.R.E. Galindo, C. Palacio, M. Henriques, A.P. Piedade, et al., Silver activation on thin films of Ag-ZrCN coatings for antimicrobial activity, Mater. Sci. Eng. C 55 (2015) 547–555, http://dx.doi.org/10.1016/j.msec.2015.05.071.
[6] R. Rebelo, R. Fangueiro, S. Carvalho, M. Henriques, S. Rana, Methods of incorporation antimicrobial agents in stents, Int. J. Eng. Sci. Innov. Technol. 3 (2014) 409–422.
[7] M.L.W. Knetsch, L.H. Koole, New strategies in the development of antimicrobial coatings: the example of increasing usage of silver and silver nanoparticles, Polymers (Basel) 3 (2011) 340–366, http://dx.doi.org/10.3390/polym3010340.
[8] R. Rebelo, N.K. Manninen, L. Fialho, M. Henriques, S. Carvalho, Morphology and oxygen incorporation effect on antimicrobial activity of silver thin films, Appl. Surf. Sci. 371 (2016) 1–8, http://dx.doi.org/10.1016/j.apsusc.2016.02.148.
[9] I. Carvalho, M. Henriques, J.C. Oliveira, C.F. Almeida Alves, A.P. Piedade, S. Carvalho, Influence of surface features on the adhesion of *Staphyloccocus epidermidis* to Ag–TiCN thin films, Sci. Technol. Adv. Mater. 14 (2013) 1–10, http://dx.doi.org/10.1088/1468-6996/14/3/035009.
[10] P. Dallas, V.K. Sharma, R. Zboril, Silver polymeric nanocomposites as advanced antimicrobial agents: classification, synthetic paths, applications, and perspectives, Adv. Colloid Interf. Sci. 166 (2011) 119–135, http://dx.doi.org/10.1016/j.cis.2011.05.008.

[11] O. Akhavan, E. Ghaderi, Capping antibacterial Ag nanorods aligned on Ti interlayer by mesoporous TiO2 layer, Surf. Coat. Technol. 203 (2009) 3123–3128, http://dx.doi.org/10.1016/j.surfcoat.2009.03.033.
[12] D.-H. Song, S.-H. Uhm, S.-B. Lee, J.-G. Han, K.-N. Kim, Antimicrobial silver-containing titanium oxide nanocomposite coatings by a reactive magnetron sputtering, Thin Solid Films 519 (2011) 7079–7085, http://dx.doi.org/10.1016/j.tsf.2011.01.385.
[13] W.M.P.F. Bosman, B.L.S. Borger van der Burg, H.M. Schuttevaer, S. Thoma, P.P. Hedeman Joosten, Infections of intravascular bare metal stents: a case report and review of literature, Eur. J. Vasc. Endovasc. Surg. 47 (2014) 87–99, http://dx.doi.org/10.1016/j.ejvs.2013.10.006.
[14] B. Reidy, A. Haase, A. Luch, K.A. Dawson, I. Lynch, Mechanisms of silver nanoparticle release, transformation and toxicity: a critical review of current knowledge and recommendations for future studies and applications, Materials (Basel) 6 (2013) 2295–2350, http://dx.doi.org/10.3390/ma6062295.
[15] J.J. Hu, C. Muratore, A.A. Voevodin, Silver diffusion and high-temperature lubrication mechanisms of YSZ-Ag-Mo based nanocomposite coatings, Compos. Sci. Technol. 67 (2007) 336–347, http://dx.doi.org/10.1016/j.compscitech.2006.09.008.
[16] D. He, A.M. Jones, S. Garg, A.N. Pharm, T.D. Waite, Silver nanoparticle–reactive oxygen species interactions: application of a charging–discharging model, J. Phys. Chem. C 115 (2011) 5461–5468, http://dx.doi.org/10.1021/jp111275a.
[17] R. Snyders, M. Wautelet, R. Gouttebaron, J.P. Dauchot, M. Hecq, Experimental and theoretical studies of the DC reactive magnetron sputtering deposition of silver oxide thin films, Surf. Coat. Technol. 174 -175 (2003) 1282–1286. doi:http://dx.doi.org/10.1016/S0257-8972.
[18] J.F. Pierson, C. Rousselot, Stability of reactively sputtered silver oxide films, Surf. Coat. Technol. 200 (2005) 276–279, http://dx.doi.org/10.1016/j.surfcoat.2005.02.005.
[19] G.A. Kumar, M.V.R. Reddy, K.N. Reddy, Structural and optical properties of AgO thin films grown by RF reactive magnetron sputtering technique, Int. Conf. Adv. Nanomater. Emerg. Eng. Technol. 2013, pp. 354–356.
[20] N.R.C. Raju, K.J. Kumar, A. Subrahmanyam, Physical properties of silver oxide thin films by pulsed laser deposition: effect of oxygen pressure during growth, J. Phys. D. Appl. Phys. 42 (2009) 135411–135416, http://dx.doi.org/10.1088/0022-3727/42/13/135411.
[21] U.K. Barik, S. Srinivasan, C.L. Nagendra, A. Subrahmanyam, Electrical and optical properties of reactive DC magnetron sputtered silver oxide thin films: role of oxygen, Thin Solid Films 429 (2003) 129–134, http://dx.doi.org/10.1016/S0040-6090(03)00064-6.
[22] D. Dellasega, A. Facibeni, F. Di Fonzo, V. Russo, C. Conti, C. Ducati, et al., Nanostructured high valence silver oxide produced by pulsed laser deposition, Appl. Surf. Sci. 255 (2009) 5248–5251.
[23] J.F. Pierson, D. Wiederkehr, A. Billard, Reactive magnetron sputtering of copper, silver, and gold, Thin Solid Films 478 (2005) 196–205, http://dx.doi.org/10.1016/j.tsf.2004.10.043.
[24] W. Wei, X. Mao, L.a. Ortiz, D.R. Sadoway, Oriented silver oxide nanostructures synthesized through a template-free electrochemical route, J. Mater. Chem. 21 (2011) 432–438, http://dx.doi.org/10.1039/c0jm02214d.
[25] A.M. Ferraria, A.P. Carapeto, A.M.B. Do Rego, X-ray photoelectron spectroscopy: silver salts revisited, Vacuum 86 (2012) 1988–1991, http://dx.doi.org/10.1016/j.vacuum.2012.05.031.
[26] C.J. Powell, Recommended Auger parameters for 42 elemental solids, J. Electron Spectrosc. Relat. Phenom. 185 (2012) 1–3, http://dx.doi.org/10.1016/j.elspec.2011.12.001.
[27] S. Calderon V, R.E. Galindo, N. Benito, C. Palacio, A. Cavaleiro, S. Carvalho, Ag^{+} release inhibition from ZrCN–Ag coatings by surface agglomeration mechanism: structural characterization, J. Phys. D. Appl. Phys. 46 (2013), http://dx.doi.org/10.1088/0022-3727/46/32/325303.
[28] I. Carvalho, M. Henriques, S. Carvalho, New strategies to fight bacterial adhesion, Microb. Pathog. Strateg. Combat. Them Sci. Technol. Educ. (2013) 170–178.
[29] J. Liu, D.A. Sonshine, S. Shervani, R.H. Hurt, Controlled release of biologically active silver from nanosilver surfaces, ACS Nano 4 (2010) 6903–6913, http://dx.doi.org/10.1021/nn102272n.
[30] S. Ninganagouda, V. Rathod, D. Singh, J. Hiremath, A.K. Singh, J. Mathew, et al., Growth kinetics and mechanistic action of reactive oxygen species released by silver nanoparticles from Aspergillus niger on *Escherichia coli*, Biomed Res. Int. 2014 (2014), http://dx.doi.org/10.1155/2014/753419.